

Low-temperature properties and magnetic ordering in Ce_2T_2In ($T = \text{Cu, Au, Pt}$)

S. Mock, A. Faisst, and H. v. Löhneysen

Physikalisches Institut, Universität Karlsruhe, D-76128 Karlsruhe, Germany

(Received 20 December 1996)

Measurements of the electrical resistivity, magnetization, susceptibility, and specific heat of Ce_2T_2In ($T = \text{Cu, Au, Pt}$) at low temperatures are reported. For $T = \text{Cu}$ and Au , antiferromagnetic order is seen below $T_N = 4.5$ and 3.6 K, respectively. For $T = \text{Pt}$, spin-glass freezing is observed below ~ 0.5 K. There is no indication of coexistence of magnetic order with heavy-fermion behavior. [S0163-1829(97)05825-6]

I. INTRODUCTION

The tetragonal CeCu_2Si_2 compound was the first heavy-fermion superconductor to be discovered.¹ Since then a large effort has been devoted to investigate the isostructural homologues $\text{Ce}T_2X_2$ where T is a transition metal or noble element and X is a polyvalent metal.² Compared to these 122 compounds, relatively little is known about 221 compounds. Recently, the synthesis of Ce_2T_2X compounds was reported.³ We have synthesized $\text{Ce}_2\text{Au}_2\text{In}$ and its Ce_2T_2In homologues ($T = \text{Cu, Pt}$) and investigated their low-temperature properties. While this work was in progress, studies with similar aim appeared.^{4,5}

II. EXPERIMENT

The polycrystalline Ce_2T_2In samples were prepared by arc melting the constituent elements (purity: Ce 3N+, Cu 5N, Au 4N, Pt 4N, In 5N) under high-purity Ar atmosphere in a water-cooled copper hearth. In order to improve homogeneity, the samples were remelted several times and subsequently annealed at 700 °C for 7 days except the Pt compound which showed a partial transformation to another structural phase upon annealing. The total mass loss after these procedures was always less than 0.1%. X-ray powder diffraction applying $\text{CuK}\alpha_1$ radiation revealed a single-phase tetragonal structure with lattice parameters $a = 8.047 \text{ \AA}$ and $c = 3.934 \text{ \AA}$ for $T = \text{Au}$ (Fig. 1). An intensity analysis of the diffraction pattern determined the structure to be of the Mo_2FeB_2 type, space group $P4/\text{mbm}$, with In on 2a, Au on 4g and Ce on 4k sites (Fig. 1). The rather large width of $\sim 0.5^\circ$ (FWHM) suggests a rather small crystallite size (diameter $\leq 10^3 \text{ \AA}$). The compounds with $T = \text{Cu}$ and Pt crystallize isostructurally, with $a = 7.728 \text{ \AA}$, $c = 3.921 \text{ \AA}$ for $T = \text{Cu}$, and $a = 7.803 \text{ \AA}$, $c = 3.880 \text{ \AA}$ for $T = \text{Pt}$. All these data are in very good agreement with previous structure determinations.

The electrical resistivity was measured on rectangular bars spark-cut from the polycrystal. Electrical contacts to current and voltage leads were made with gold paint. The magnetization was measured with a moving-sample magnetometer⁶ and in a low-field SQUID magnetometer. The specific heat was measured with the standard semiadiabatic heat-pulse method in magnetic fields up to 6 T.

III. RESULTS AND DISCUSSION

A. $\text{Ce}_2\text{Au}_2\text{In}$

Figure 2 shows the electrical resistivity $\rho(T)$ measured at temperatures T between 300 K down to 30 mK. The data below 10 K are shown in the inset. The resistivity ratio of ~ 10 signals a rather good sample quality compared to the earlier studies^{4,5} although the residual resistivity of $29 \mu\Omega \text{ cm}$ is still rather high. The most prominent features of $\rho(T)$ are (i) a pronounced shoulder slightly above 100 K which we tentatively attribute to scattering from crystal-field excitations and (ii) a sharp kink at 3.5 K. The data between 30 mK and 3.5 K can be described as $\rho(T) = \rho_0 + AT^m$ with $\rho_0 = 29 \mu\Omega \text{ cm}$, $A = 0.64 \mu\Omega \text{ cm} / \text{K}^m$, and $m = 3$. In a magnetic field $B = 7 \text{ T}$, the same functional T dependence of ρ is found, with different $A = 0.24 \mu\Omega \text{ cm} / \text{K}^m$. ρ_0 increases up to $35 \mu\Omega \text{ cm}$ which we interpret as the ordinary positive magnetoresistance (Kohler's rule). From the very large specific-heat anomaly at 3.5 K (see below) we can rule out that the kink in $\rho(T)$ arises from minute amounts of elemental In (superconducting transition at 3.4 K). Rather, we attribute it to the freezing of spin-order scattering because of magnetic order setting in at 3.5 K.

Figure 3 shows magnetization data taken in different fields plotted as M/B vs T . A sharp kink at 3.6 K is observed in $B = 0.1 \text{ T}$ which is rounded and shifted to lower T as B

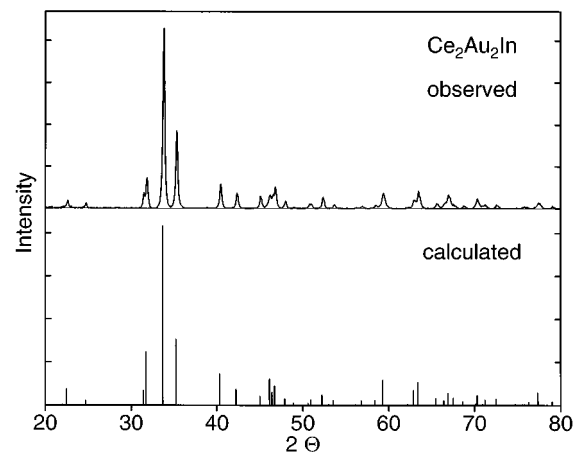


FIG. 1. Observed and calculated x-ray diffraction pattern of $\text{Ce}_2\text{Au}_2\text{In}$ ($\theta - 2\theta$ powder method). Calculation assumes the Mo_2FeB_2 structure.

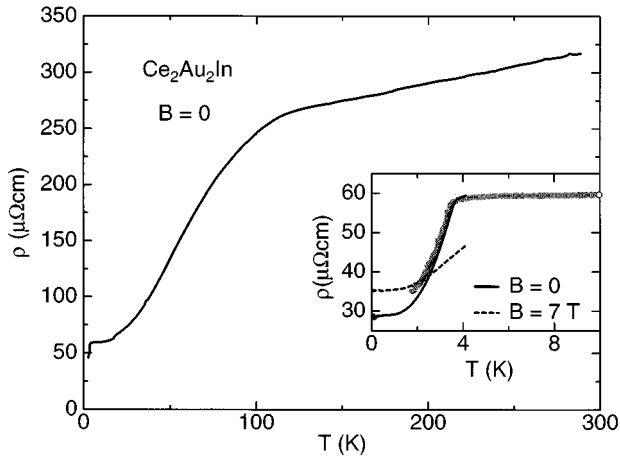


FIG. 2. Electrical resistivity ρ vs temperature T of $\text{Ce}_2\text{Au}_2\text{In}$ between 2 K and 300 K (main frame) and in the low- T range between 30 mK and 10 K (inset). Here the symbols denote the measurements in the ^4He cryostat above 2 K and the solid line indicates the data measured in the dilution refrigerator, both in zero magnetic fields. The dashed line denotes low- T data measured in 7 T.

increases, suggesting the onset of antiferromagnetic order. Throughout this paper the units of magnetization μ_B/T are for one Ce atom. We take $\max[d(\chi T)/dT]$ as the Néel temperature $T_N=3.5$ K. No feature is resolved in $B=3$ T. The rounding might be attributed to averaging over crystallite directions in our polycrystalline samples. The inset of Fig. 3 shows the dc susceptibility measured in 1 mT with a SQUID magnetometer. The data above T_N follow quite nicely a Curie-Weiss law with an effective moment $\mu_{\text{eff}}=1.8\mu_B$ and a Curie-Weiss temperature $\theta=-1$ K. The reduction of μ_{eff} with respect to the Ce^{+3} free-ion value found above 50 K (Ref. 4) is attributed to the crystal field. In the whole T range investigated no difference was seen between the zero-field-cooled and field-cooled susceptibility. We also measured magnetization curves $M(B)$ at 0.3 K and 3 K. Figure 4 shows the M vs B data, with the inset of Fig. 4 depicting dM/dB . The steplike feature in M vs B for $T=0.3$ K, i.e., a

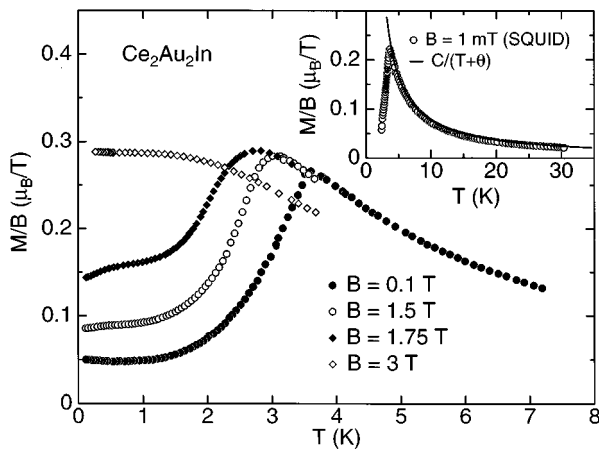


FIG. 3. Magnetization M divided by applied magnetic field B of $\text{Ce}_2\text{Au}_2\text{In}$ vs temperature T for different fields B . Inset shows the susceptibility measured for $B = 1$ mT with a SQUID magnetometer up to 30 K, together with a Curie-Weiss fit.

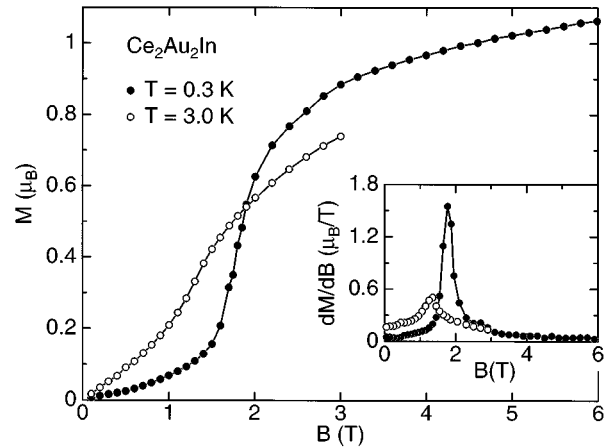


FIG. 4. Magnetization M of $\text{Ce}_2\text{Au}_2\text{In}$ vs applied magnetic field B for temperatures $T=0.3$ and 3 K. The inset shows dM/dB vs T .

sharp maximum in dM/dB , indicates the transition from the antiferromagnetic to the paramagnetic phase. A maximum in dM/dB is still visible at 3 K, as has been found before at 1.7 K.⁴

Figure 5 shows the specific heat C between 50 mK and 10 K. Throughout this paper 1 mol corresponds to 1 mol of Ce atoms or, equivalently, 1/2 formula units. The very sharp maximum at $T_N=3.5$ K in zero magnetic field is in very good agreement with T_N determined from the magnetization and supports the notion of a magnetic phase transition (a superconducting transition of possible In precipitations would be invisible on this plot). The sharp zero-field transition widens and shifts to lower T in a magnetic field of 1.5 T. Actually, two transitions are suggestive through the wide and clearly nonmonotonic slope of the specific heat just above the maximum. For 3 T, three rather sharp features are observed and for 6 T, only one transition at 2.5 K is seen. These results differ somewhat from the specific-heat study of Hauser *et al.*⁵ where only one maximum was observed for fields up to 3 T, and none above 2.4 K for 6 T. The obvious explanation for the observation of two features is that we

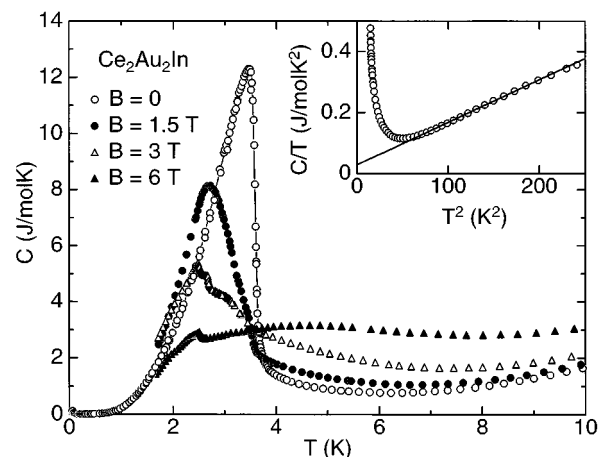


FIG. 5. Specific heat C of $\text{Ce}_2\text{Au}_2\text{In}$ vs temperature T in various applied magnetic fields B . Inset shows C/T vs T^2 at high temperatures.

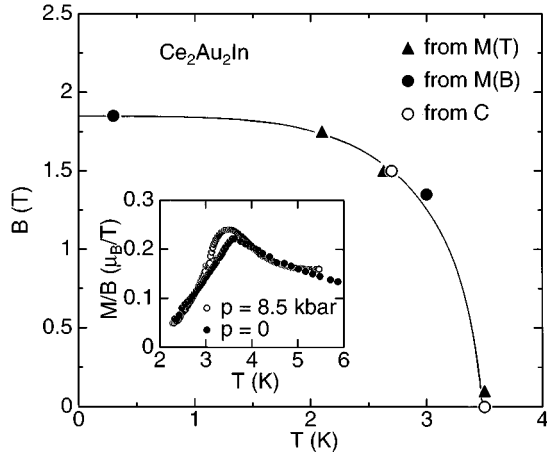


FIG. 6. Magnetic phase diagram of $\text{Ce}_2\text{Au}_2\text{In}$, presumably for B along the easy direction, as determined from magnetization M and specific heat C . The inset displays the pressure dependence of M/B around T_N .

observe transitions of differently oriented grains of our polycrystal with respect to the field direction, similar to the case of the magnetization. However, the specific heat picks also the hard directions for which T_N does not decrease quickly with increasing field. This is different from the magnetization where grains with their easy direction parallel to the field contribute much stronger to M than those with the hard direction parallel to B , at least in the paramagnetic state. The magnetic phase diagram of $\text{Ce}_2\text{Au}_2\text{In}$ (presumably for the easy direction) is shown in Fig. 6. It exhibits the “typical” mean-field-like phase line between antiferromagnetic and paramagnetic state.

It is interesting to note that even for this polycrystalline alloy a rather narrow “crossing region” where all the C/T curves for different fields cross each other is found. This universal crossing has been recently related to other thermodynamic properties of magnetic materials.⁷

The inset of Fig. 5 shows the data between 10 K and 15 K plotted as C/T vs T^2 . From the slope $\beta = 1.39$ mJ/mol K⁴ we infer a Debye temperature θ_D of 151 K. The value of β (and θ_D) is an upper (lower) bound because crystal-field excitations may also contribute to C in this T range. Furthermore, the data above 15 K show negative deviations from the T^3 dependence due to onset of phonon dispersion. The Sommerfeld coefficient for this high- T region is rather low, $\gamma_{\text{HT}} = (28 \pm 5)$ mJ/mol K². However, we cannot exclude that the rise of C with decreasing T in the range just above T_N arises from the Kondo effect with a Kondo temperature of a few K. The intervening antiferromagnetic transition prevents a definite conclusion. Figure 7 shows the specific heat $C(T)$ as measured between 50 mK and 30 K on a log-log scale to highlight the low- T data. At lowest T , a $b_N T^{-2}$ dependence is observed which presumably arises from the quadrupolar splitting of In nuclei with noncubic site symmetry. The inset shows the data below 0.4 K plotted as CT^2 vs T^3 where the slope yields $\gamma_{\text{LT}} = 37$ mJ/mol K². This small γ_{LT} value is of the same order as γ_{HT} . Above ~ 0.4 K, C increases more rapidly than linearly. In the whole region up to 1.5 K the data can be described by $C = b_N T^{-2} + \gamma_{\text{LT}} T + \beta_M T^3 \exp(-\Delta E/k_B T)$ with $b_N = 0.38$ mJ K/mol,

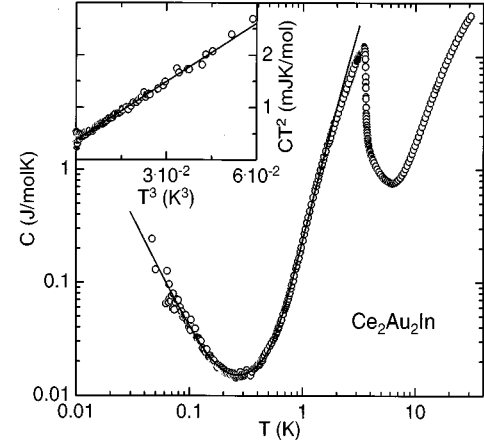


FIG. 7. Specific heat C vs temperature T of $\text{Ce}_2\text{Au}_2\text{In}$ on a log-log plot. Solid line is a fit of $C = b_N T^{-2} + \gamma_{\text{LT}} T + \beta_M T^3 \exp(-\Delta E/k_B T)$ to the data. The inset shows CT^2 vs T^3 to determine b_N and γ_{LT} .

$\beta_M = 0.95$ J/mol K⁴ and $\Delta E/k_B = 1.56$ K. The latter term is expected for an anisotropic antiferromagnet.

There is no indication for a strong Kondo effect in the presence of antiferromagnetic order in $\text{Ce}_2\text{Au}_2\text{In}$. First, the total entropy associated with the specific-heat anomaly at T_N (acquired between 0.4 K and 7 K to incorporate short-range-order effects above T_N) is $\sim 90\%$ of $R \ln 2$. Second, there is no evidence for a sizable linear specific-heat term $\gamma_{\text{LT}} T$. Third, the magnetization at 0.3 K reaches $1.05 \mu_B$ in 6 T which is not too far away from the effective moment $\mu_{\text{eff}} = 1.8 \mu_B$ determined from the Curie-Weiss fit (inset of Fig. 3).

Finally, the inset of Fig. 6 shows the pressure dependence of χ in the vicinity of T_N . For the measurement in 8.5 kbar, the sample was inserted into a standard CuBe pressure cell with a methanol/ethanol mixture as pressure-transmitting medium. The magnetic signal of the empty cell was determined in a separate run and subtracted from the data. The pressure was obtained by measuring simultaneously the superconducting transition of two small Pb samples inside and outside of the cell. The antiferromagnetic transition for 8.5 kbar is rather broad possibly due to nonhydrostatic pressure. Nevertheless a clear downward shift of T_N is observed, similar in magnitude to the observation of Hauser *et al.*⁵ from resistivity measurements under pressure.

B. $\text{Ce}_2\text{Cu}_2\text{In}$

Figure 8 shows the electrical resistivity $\rho(T)$ of $\text{Ce}_2\text{Cu}_2\text{In}$. Overall similar behavior to $\rho(T)$ of $\text{Ce}_2\text{Au}_2\text{In}$ is found, with a shoulder at 100 K and a rather sharp kink at 5 K, signaling crystal-field excitations and magnetic order, respectively. These findings again correspond to earlier reports.^{4,5} The magnetization data are shown in Fig. 8. Figure 9 shows the dc susceptibility measured up to 40 K. The data above T_N can be described by a Curie-Weiss fit with $\mu_{\text{eff}} = 1.95 \mu_B$ and $\theta = +1.8$ K. The positive sign of θ suggests strong antiferromagnetic interactions, in line with a larger Néel temperature $T_N = 4.7$ K [again as determined from $d(\chi T)/dT$] compared to that of $\text{Ce}_2\text{Au}_2\text{In}$. The coin-

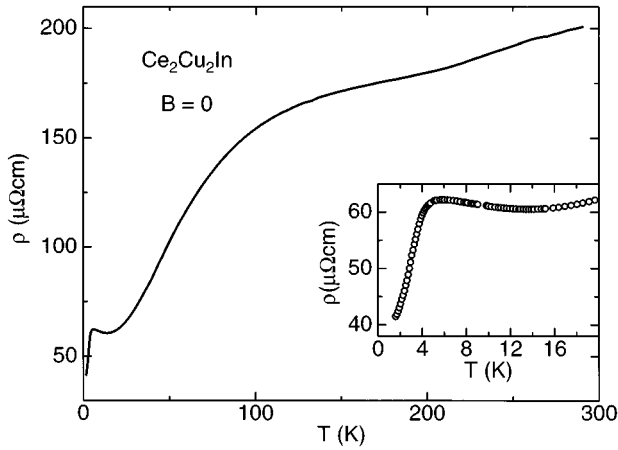


FIG. 8. Electrical resistivity ρ vs temperature T of $\text{Ce}_2\text{Cu}_2\text{In}$. The inset shows the data between 1.5 and 20 K on an expanded scale.

vidence of a smaller unit-cell volume with larger T_N again suggests that there is only a weak Kondo effect in this class of materials. The effective exchange interaction between $4f$ electrons and conduction electrons J is rather small, i.e., the Ce moments are quite stable, and any decrease in the lattice constants leads to an increase of J and thus favors the RKKY amplitude $J^2N(E_f)$ where $N(E_f)$ is the density of states at the Fermi level, over the exponentially small Kondo effect. Nevertheless, the increase of $\rho(T)$ above T_N towards low T may be due to the Kondo effect as suggested before.⁴ Also shown in Fig. 9 is the dc magnetization as measured in $B=0.1$ T down to ~ 0.1 K which is in reasonably agreement ($\sim 10\%$) with the SQUID data in the region of overlap. The inset shows $M(B)$ measured at 0.3 K indicating the transition from antiferromagnetic to paramagnetic state, much like in $\text{Ce}_2\text{Au}_2\text{In}$ (cf. Fig. 4) although in $\text{Ce}_2\text{Cu}_2\text{In}$ the transition is much wider and exhibits some fine-structure.

Figure 10 shows the specific heat of $\text{Ce}_2\text{Cu}_2\text{In}$. Here a strong difference between annealed and unannealed samples is observed. The latter shows two distinct features, i.e., a kink at 5.6 K and a maximum at 4.6 K, signaling a “double transition” as already observed by Hauser *et al.*⁵ These au-

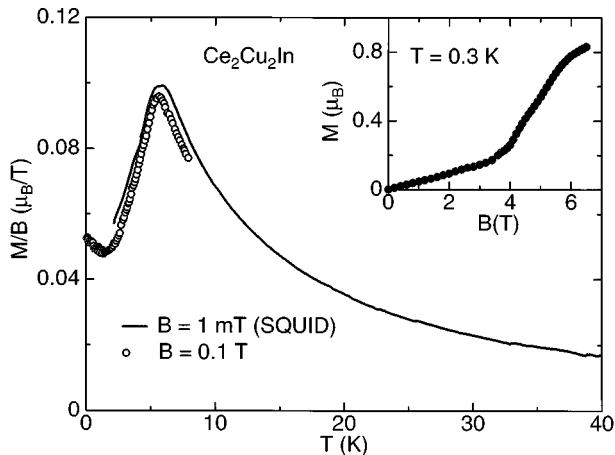


FIG. 9. M/B of $\text{Ce}_2\text{Cu}_2\text{In}$ vs T as measured in 0.1 T and 1 mT. The inset shows the magnetization curve $M(B)$ at 0.3 K.

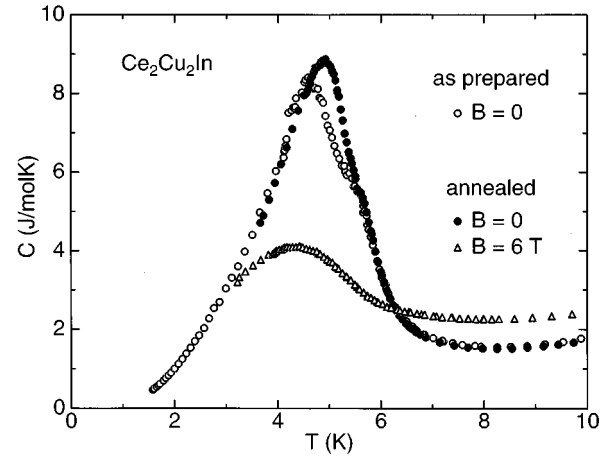


FIG. 10. Specific heat C of $\text{Ce}_2\text{Cu}_2\text{In}$ vs temperature T of an as-prepared sample for $B=0$ and of the same sample after annealing for $B=0$ and 6 T.

thors do not report on the sample treatment. For the annealed sample, the maximum has shifted upward to 4.9 K and the kink has almost disappeared. In 6 T, only a broad maximum located around 4.5 K remains. Due to the relatively high T_N a reliable determination of γ_{HT} from a C/T vs T^2 plot was not possible.

C. $\text{Ce}_2\text{Pt}_2\text{In}$

The electrical resistivity $\rho(T)$ of $\text{Ce}_2\text{Pt}_2\text{In}$ is shown in Fig. 11. We observe no low- T feature which might indicate a magnetic-phase transition, but the crystal-field related anomaly is still present. It is actually shifted to somewhat lower temperatures compared to the other two homologues. The resistivity at 300 K is rather low compared to the other homologues and also to the previous reports.^{4,5} The inset shows the low- T data. As noted before,⁴ $\rho(T)$ does not follow a T^2 dependence. Figure 12 shows the magnetization divided by the applied field, M/B , for $B=0.1$ T in the region up to 7 K. χ as measured in 1 mT up to 30 K yields $\mu_{\text{eff}}=0.94\mu_B$ and $\theta=-1$ K from a Curie-Weiss fit (not shown). No indication of magnetic order is seen above 1 K,

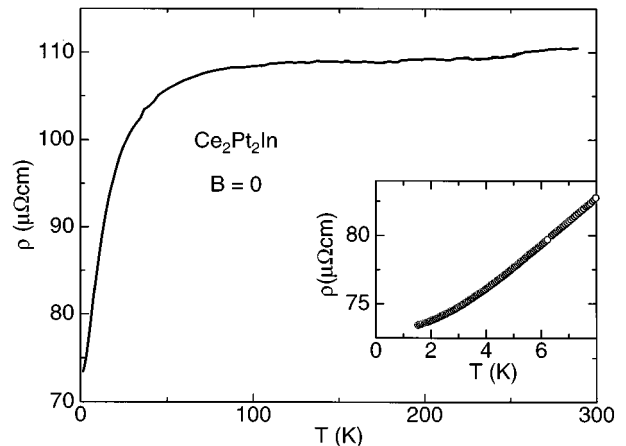


FIG. 11. Electrical resistivity ρ vs T of $\text{Ce}_2\text{Pt}_2\text{In}$. The inset shows the low- T data.

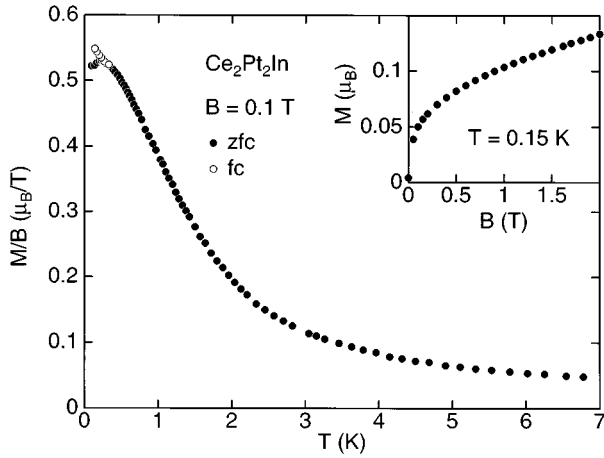


FIG. 12. M/B of $\text{Ce}_2\text{Pt}_2\text{In}$ vs T for applied magnetic field $B=0.1$ T after zero-field cooling (ZFC) and field cooling (FC). The inset shows the magnetization curve $M_{\text{ZFC}}(B)$ at 0.15 K.

as already pointed out previously by Hauser *et al.*⁵ However, a quite unusual behavior is observed in the low-temperature magnetization. Figure 13 shows M/B in the region below 1 K in detail. M/B is seen to split into zero-field-cooled (ZFC) and field-cooled (FC) branches as indicative of a spin glass, with a maximum in the ZFC curve and a continuous increase of the FC curve towards lower temperatures. The splitting occurs at lower T for higher fields. The ac susceptibility χ^{ac} shows a maximum at $T=0.55$ K. What is unusual, however, is that FC and ZFC M/B curves in small fields (1 and 10 mT) differ even well above the “freezing temperature” [taken as the maximum of $M_{\text{ZFC}}(T)$]. In concordance with this finding is the strongly nonlinear behavior of M/B even for small fields and temperatures up to 1 K (cf. Fig. 13). The inset of Fig. 12 shows $M_{\text{ZFC}}(B)$ measured at 0.15 K.

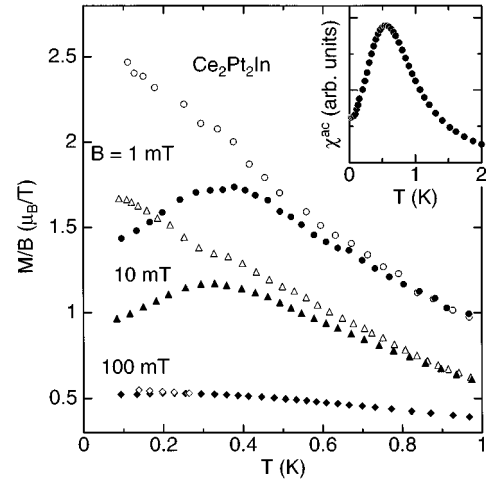


FIG. 13. M/B of $\text{Ce}_2\text{Pt}_2\text{In}$ vs T in the temperature range below 1 K, showing the difference between field-cooled (open symbols) and zero-field-cooled (closed symbols) magnetization in different fields. The inset shows the ac susceptibility measured in $B \sim 10^{-5}$ T.

Surprisingly, M attains only $0.13\mu_B$ in 2 T. In view of this unusual behavior, the rather large linear specific-heat term $\gamma \sim 0.5$ J/mol K^2 inferred from the data above 1 K (Ref. 5) might be attributed to the spin-glass properties of $\text{Ce}_2\text{Pt}_2\text{In}$ and probably is not a manifestation of a Kondo-lattice effect in terms of heavy quasiparticles.

ACKNOWLEDGMENTS

We thank B. Kübler, T. Pietrus, U. Tutsch, and R. Vollmer for performing some low-temperature measurements. This work was supported by the Deutsche Forschungsgemeinschaft and by the Ministerium für Wissenschaft und Forschung Baden-Württemberg.

¹F. Steglich, J. Aarts, C. D. Bredl, W. Lieke, D. Meschede, W. Franz, and H. Schäfer, Phys. Rev. Lett. **43**, 1892 (1979).

²For a review see, e.g., Conference Proceedings of the International Conferences on Strongly Correlated Electron Systems [Physica B **199&200** (1994); **206&207** (1995); **223&224** (1996)].

³F. Hulliger and B. Z. Xue, J. Alloys Compd. **215**, 267 (1994); F. Hulliger, *ibid.* **217**, 1648 (1995); **221**, 211 (1995); R. A. Gordon,

Y. Ijivi, C. M. Spencer, and F. J. DiSalvo, *ibid.* **224**, 101 (1995).

⁴D. Kaczorowski, P. Rogl, and K. Hiebl, Phys. Rev. B **54**, 9891 (1996).

⁵R. Hauser, H. Michor, E. Bauer, G. Hilscher, and D. Kaczorowski, Physica B (to be published).

⁶H. G. Schlager, A. Schröder, M. Welsch, and H. v. Löhneysen, J. Low Temp. Phys. **90**, 181 (1993).

⁷D. Vollhardt, Phys. Rev. Lett. **78**, 1307 (1997).